# *Storm surge risks and associated synoptic patterns for the great slave lake shoreline*

Results in Engineering 31 (2026) 111612

Contents lists available at ScienceDirect

Results in Engineering

journal homepage: www.sciencedirect.com/journal/results-in-engineering

Research paper

# Storm surge risks and associated synoptic patterns for the Great Slave Lake shoreline

Boyuan Yu [a,*], Shinto Roose [a], Laxmi Sushama [a], Teufel Bernardo [b], Ram Yerubandi [b]

[a] Department of Civil Engineering and Trottier Institute for Sustainability in Engineering and Design, McGill University, Montreal, Canada
[b] Water Science and Technology Division, Environment and Climate Change Canada, Canada

ARTICLE INFO

*Keywords:*
Storm surge
Climate change
Great Slave Lake
Synoptic patterns

ABSTRACT

This study assesses storm surge characteristics for the Great Slave Lake region situated in the Northwest Territories of Canada for current (1991-2020) and future (2041-2070) climates for the SSP5-8.5 scenario. Coupled hydrodynamic-wave simulations, performed for extreme storm events corresponding to archetypal synoptic patterns identified using structural self-organizing maps applied to mean sea level pressure fields from high-resolution regional climate model simulations, are used to assess surge levels for the shoreline regions. Results for the current period indicate that the southern shorelines of the basin experience surge levels of up to 0.6 m, primarily linked to synoptic patterns characterised by strong westerly and northwesterly winds over the lake. In contrast, the northern shoreline experiences relatively low surge. Future projections indicate intensification of northwesterly, westerly, and northeasterly winds, further enhancing surge levels for the southern shores, with 22% and 59% increases projected for the communities of Fort Resolution and Hay River, respectively. Potential increase in storm surge is also projected for the east arm, including the Łutselk'e community. Although the frequency of synoptic patterns linked to southwesterly winds impacting northern shorelines is projected to increase by 46%, the relatively smaller changes in wind magnitude yield no substantial changes in surge levels for the northern shorelines, including Yellowknife. Although surge levels are relatively small compared to oceanic coastline regions, the high vulnerability of these remote regions necessitates detailed quantification of risks to support development of adaptation strategies to ensure climate resiliency of shoreline infrastructure and communities.

## 1. Introduction

Storm surges and associated inundation pose significant threats to both human life and infrastructure. A storm surge is characterized by an abnormal rise in water level above predicted astronomical tide, driven by variations in atmospheric pressure and associated winds. In a changing climate, sea level rise, and more intense storms are expected to increase the severity of storm surges [1]. In addition to storm size, intensity, central pressure, timing of storm relative to tidal phase and orientation of the storm with respect to the shoreline, regional factors such as local bathymetry, coastline shape and topography determine the amplitude of a storm surge at any given coastal region [2,3]. Tropical storms, extratropical storms, and mixed systems such as tropical storms undergoing extratropical transition can all generate large storm surges and flooding [4–6]. The deadliest and highest recorded storm surges ever recorded have been associated with tropical storms [7]. Extreme extratropical storms can cause storm surges in the mid- and high-latitude regions [8]. These storm systems are expected to both intensify and extend in spatial scale under global warming, according to multi-climate model projections [9].

Studies thus far have mostly focused on storm surges in the context of oceanic coastlines [10–13]. Commonly used hydrodynamic models for storm-surge simulation are based on finite volume methods [14–16] and finite element methods [17–21]. Coupling hydrodynamic model with spectral-wave model has demonstrated to improve the prediction of storm surge levels due to their ability in capturing small-scale physical processes into account, such as white capping, wave breaking and wave-wave interaction. For instance, Dietrich et al. [22] using ADCIRC (ADvanced CIRCulation; Westerink et al. [21]) and SWAN (Simulating WAves Nearshore; [23]) for Hurricanes Katrina and Rita at Gulf of Mexico, Warner et al. [16] and Roland et al. [24] using ROMS (Regional Ocean Modelling System; [25]) coupled to SWAN and SELFE

* Corresponding author.
*E-mail address:* boyuan.yu@mail.mcgill.ca (B. Yu).

https://doi.org/10.1016/j.rineng.2026.111612
Received 18 February 2026; Received in revised form 7 May 2026; Accepted 17 June 2026
Available online 17 June 2026

(Semi-implicit Eulerian–Lagrangian finite-element model; [19]) coupled to WWM-II (second-generation Wind Wave Model) for Hurricane Isabel at the mid-Atlantic Bight region on U.S. East Coast, respectively, demonstrated that the coupled hydrodynamic-wave simulation improves surge level compared with the standalone hydrodynamic simulation. Similar results were also obtained by the coupled simulation of SCHISM (Semi-implicit Cross-scale Hydroscience Integrated System Model; [20]) and WWM-III (third-generation Wind Wave Model) performed by Hsiao et al. [26] and Chang et al. [27] for the case of super typhoons in the South China Sea.

The methods commonly used to evaluate the impact of storm surges are the return-level-based and event-based approaches. In the return-level-based approach, the total water elevation at the point of interest is obtained based on the frequency analysis of wave setups, storm surges and tides [28,29]. The event-based approach on the other hand considers the extreme storm events to inform hydrodynamic simulations [16,22,24].

Although some previous works have looked at storm surges in large lakes [30,31], relevant studies are still limited. In Canada, studies have generally focussed on the Laurentian Great Lakes. Storm-surge hazards for large lakes in the Canadian high-latitude regions such as the Great Slave Lake (GSL) have received relatively less attention. During the ice-free periods, storm surges in high-latitude inland lakes can be triggered by intense frontal systems, namely mid-latitude cyclones, characterized by strong warm and cold fronts. The frequency of these storms may decrease according to Hoskins and Woollings [32], as accelerated Arctic warming projected for future warmer climate weakens meridional temperature gradients, reducing low-level baroclinicity and weakening the thermally driven jet. This reduction in baroclinicity leads to weaker growth rates of baroclinic disturbances and thereby weaker midlatitude cyclogenesis. However, recent studies such as Gentile et al. [33,34] suggest that the percentage of storms linked to extreme wind events is predicted to increase in a warmer climate, although the overall number of midlatitude storms is predicted to decline. Storm surges can therefore be expected to lead to higher wave runup and flooding along the shorelines of large lakes in these northern regions [35,36]. Although the storm surge magnitudes can be smaller compared to the oceanic context, the high vulnerability of the northern lake communities necessitate an in-depth understanding of storm surge characteristics to ensure coastline infrastructure protection and the safety of communities [37,38].

Research for GSL has so far mainly focused on lake water budget [39,40], meteorological characteristics [41–44], seasonal stratification and ventilation [45–47], and ice phenology [43,45,48–50]. Systematic studies focussed on wave and storm surge characteristics are lacking for this region, for current and future climates, despite the apparent socio-economic significance. This study, therefore, using a coupled hydrodynamic-wave model, informed by regional climate model (RCM) simulations for current and future climates, for the first time, assesses shoreline vulnerabilities from storm surge perspective under a warming climate.

The rest of the paper is organized as follows. The methodology used for identifying typical synoptic patterns for the GSL region and undertaking hydrodynamic-wave simulations are presented in Section 2. Sections 3 and 4 present results for synoptic and storm surge characteristics for current and future climates, respectively. Discussion, and conclusions are presented in Sections 5 and 6, respectively.

## 2. Methodology

An event-based approach is used in this study to identify vulnerabilities of the GSL shorelines to combined storm surge and surface wave effects. To this end, extreme wind events corresponding to typical synoptic patterns for the GSL region (53°N to 66.5°N and 126°W to 98°W) for the ice-free period, spanning from June to November, for the current 1991–2020 period are identified using outputs from the Global Environmental Multiscale (GEM) model simulation [51], driven by European Centre for Medium-Range Weather Forecasts (ECMWF) fifth-generation reanalysis product ERA5 [52] at the lateral boundaries (referred to as GEM_ERA5 hereafter). The synoptic patterns for the GSL region are identified using structural self-organizing maps (SOM; [53]), an unsupervised artificial neural network method, applied to mean sea level pressure (MSLP) data from GEM_ERA5 over the analysis domain covering the GSL region shown in Fig. 1(a). To ensure that the synoptic patterns rather than localized, short-lived variations are captured, smoothed six hourly MSLP is considered for SOM analysis. Structural SOM produces more reliable and physically meaningful classification of synoptic types than typical SOM algorithms by preserving the underlying spatial properties of meteorological patterns [53].

Coupled hydrodynamic-wave simulations for the extreme wind/storm events corresponding to identified typical patterns, considered as the maximum of hourly wind magnitudes grouped by synoptic pattern, are employed to simulate combined storm surge and wave effects to identify impacted shoreline sections. Delft3D [15] and SWAN [23] are the hydrodynamic and wave models considered. The hydrodynamic model transfers information of water level and current velocity to the spectral wave model, while the spectral-wave model provides the wave-radiation stress to the hydrodynamic model as a source term in the momentum equation. Detailed formulation of these models can be found under Supplementary Material. The bathymetry of GSL considered in the hydrodynamic simulation is shown in Fig. 1(b), which is obtained from Schertzer [54] and Environment and Climate Change Canada (personal communication). The main west basin of GSL is moderately deep with maximum depth of 163 m, while the east arm is deeper, with a maximum depth of 614 m at Christie Bay. Fig. 1(c) shows the unstructured grid used for coupled hydrodynamic-wave simulation. Higher resolution of 250 m is used to better resolve irregular shorelines and regions of sharp bathymetry gradients, while coarser resolution of up to 1000 m is used elsewhere.

Validation of GEM_ERA5 simulated wind and synoptic patterns and Delft3D-SWAN simulated surge levels and significant wave heights are performed to assess the ability of the models such that they can be applied in future simulations. Wind and synoptic characteristics are compared against ERA5 data for the 1991-2020 period. Hourly observed wind data from Environment and Climate Change Canada (ECCC) at four selected locations (Yellowknife, Łutselk'e, Fort Resolution and Hay River) are also considered for validating GEM_ERA5 simulated wind fields for the 2014 to 2020 observation period. Water levels are validated with observed data available at Yellowknife Bay (62.4°N 114.3°W) station, and significant wave heights against those at two buoy stations – C45141 (61.2°N 115.3°W) and C45150 (62.0°N 114.1°W) – maintained by ECCC [55], which are shown in Fig. 1(b).

Vulnerability of the shorelines to combined storm surge and wave effects in future climate are assessed using a similar approach, but using data from a transient climate change GEM simulation spanning the 1991-2070 period, driven by the Max Planck Institute Earth System Model 1.2 (MPI-ESM1-2-HR) at the lateral boundaries (referred to hereafter as GEM_MPI), for the Shared Socioeconomic Pathway scenario SSP5-8.5. This scenario enables the assessment of a worst-case climate change trajectory characterized by high greenhouse gas emissions [56]. The wind and synoptic patterns simulated by GEM_MPI for the current 1991-2020 period are compared to those of GEM_ERA5 to understand the boundary forcing errors, i.e. errors in GEM_MPI simulation stemming from errors in the driving MPI-ESM1-2-HR data, which help identify regions needing cautionary interpretation of projected changes. Projected changes to the frequency of typical synoptic patterns, magnitude of extreme wind events for each synoptic pattern and related combined storm surge-wave impacts are assessed for the 2041-2070 period with respect to the 1991-2020 period. The schematic representation of the methodology in the form of a flowchart is shown in Fig. 2.

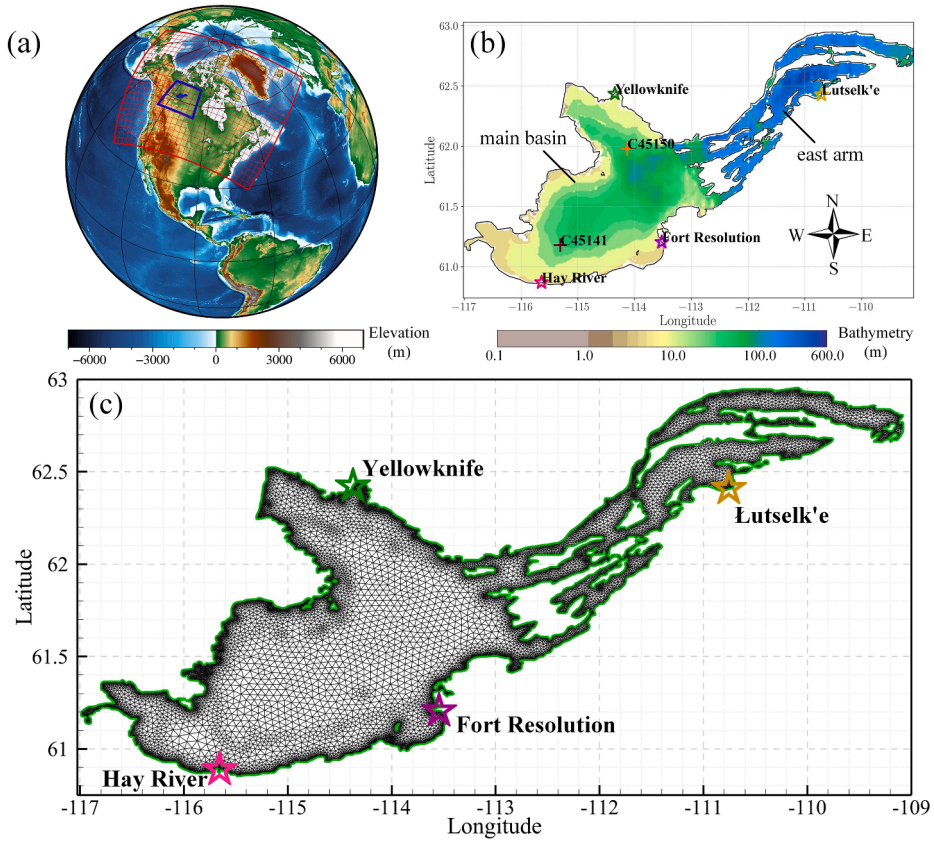


**Fig. 1.** (a) The experimental domain of the Global Environment Multiscale model (GEM) at 0.11° resolution; every 20th grid point is shown. The blue rectangle centered over for Great Slave Lake (GSL) represents the analysis domain considered for SOM analysis. (b) Bathymetry of GSL. The location of four communities (Yellowknife, Hay River, Fort Resolution and Łutselk'e) situated along the shorelines of GSL are denoted with star symbols, and the two buoy observation stations are denoted with crosses. (c) The unstructured grid configuration considered for the coupled hydrodynamic-wave simulation for GSL, with fine resolution of 250 m closer to the shoreline and coarser resolution of up to 1000 m elsewhere.

## 3. Typical synoptic and combined storm surge - wave patterns in current climate

### 3.1. Typical synoptic patterns

To establish confidence in the climate model, the ability of GEM_ERA5 in capturing surface wind characteristics relevant to storm and low-pressure systems for the ice-free study period (summer - JJA and Fall - SON) are first evaluated over the analysis domain. During summer, the mean surface winds are dominated by northeasterlies over the GSL, while in fall the region experiences southwesterlies in the south and northeasterlies in the north, both of which are well captured by GEM_ERA5 (Fig. 3). While GEM_ERA5 simulations closely match the large-scale seasonal wind patterns in the ERA5 dataset over the GSL region (Fig. 3), hourly station observations are also used to validate the model performance. This ensures that the simulations capture both the shorter timescales of local wind pattern and large-scale seasonal variability.

Comparison of observed and GEM_ERA5-based wind roses (Figure S1) at four locations – Yellowknife, Fort Resolution, Hay River and Łutselk'e – indicate that the observed wind patterns are reasonably well captured by GEM_ERA5. At Yellowknife, observations show that winds are dominated by easterlies, primarily due to the weather systems passing from west to east [57] and winds are rarely from southwest among other directions. GEM_ERA5 captures these patterns realistically. At Łutselk'e, observed winds are predominantly northeasterly or westerly and with few occurrences from other directions [58]. GEM_ERA5 reproduces the observed patterns at both Yellowknife and Łutselk'e, although it tends to overestimate wind magnitudes. At Fort Resolution, observations indicate dominant northwesterly and southeasterly winds. GEM_ERA5 captures the dominant wind directions but underestimates their magnitudes compared to observations. The spatial pattern of summer winds shows strong observed northeasterlies across GSL, directed toward Hay River (Fig. 3). At this location, surface winds are predominantly onshore, driven by a northeasterly lake breeze during summer, while stronger northwesterly and southeasterly winds become more frequent in fall [58]. These observed features are also well captured by the GEM_ERA5 simulation. The channelling effect of the Mackenzie River Valley drives northwesterly winds at Hay River year around [57], which GEM_ERA5 reproduces. Overall, the observed patterns are reasonably represented by GEM_ERA5, even though GEM_ERA5-based wind roses are for representative grid cells of 10 km resolution. GEM_ERA5 wind roses are more similar to those based on ERA5 compared to those observed (Figure S1).

The location of the pressure systems has a significant influence on how storms affect the various GSL shorelines. Therefore, SOM analysis is conducted over the analysis domain centred over GSL to more clearly resolve the synoptic patterns that directly affect the lake shoreline regions. It must be noted though that low pressure systems entering or leaving the boundaries might only be partially represented because the domain only represents a section of the large-scale circulation. Following the methodology discussed in Section 2, eight typical SOM patterns, that reveal the orientation of pressure gradients and the spatial positioning of high- and low-pressure areas across the GSL domain, are identified for the 1991-2020 period from ERA5 and GEM_ERA5 based on the SSIM (structural similarity index); SSIM provides a quantitative measure of the degree of resemblance among the identified patterns Figure S2 depicts the SSIM values for the eight SOM patterns in

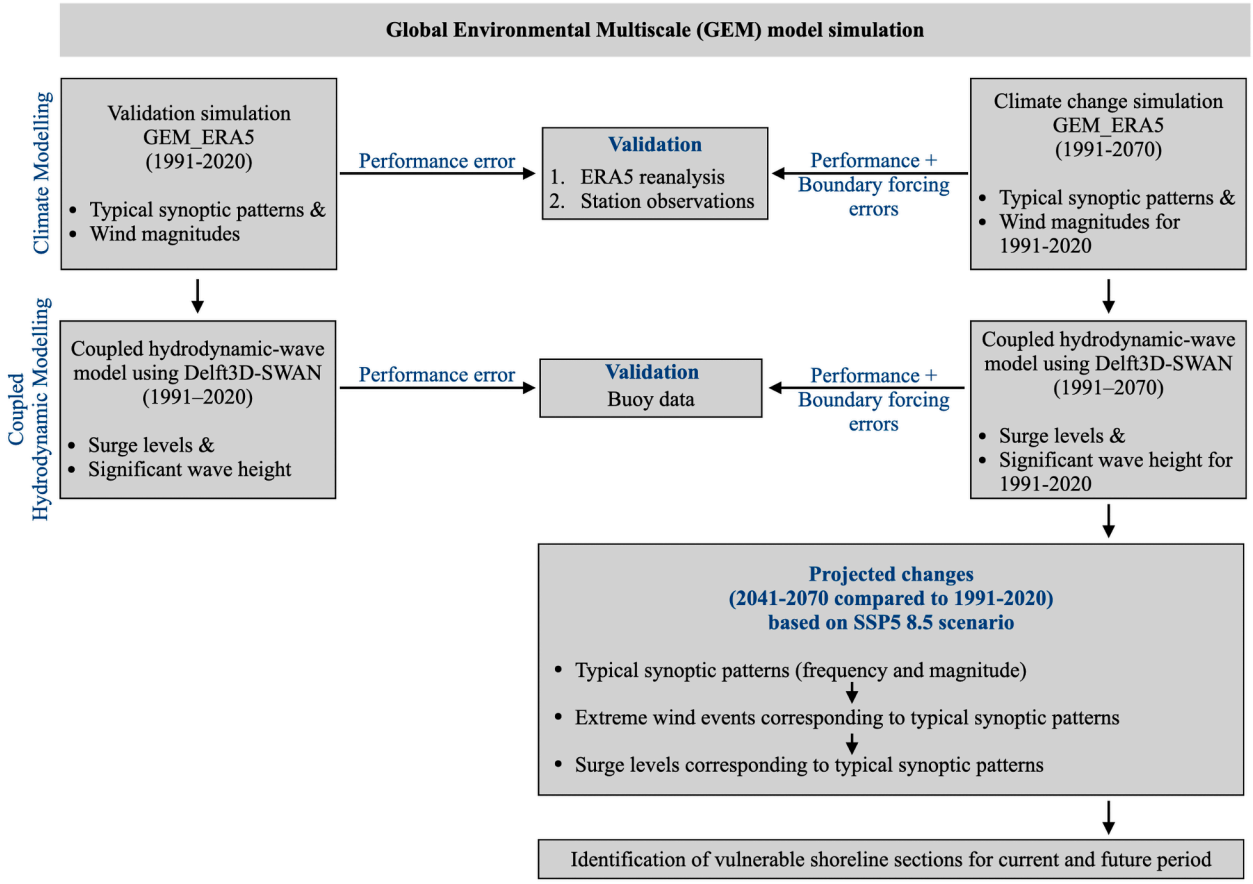


**Fig. 2.** Schematic representation of the methodology.

topological order. Adjacent patterns share a significant degree of structural similarity, as evidenced by the relatively high SSIM values of neighbouring nodes, which are usually around 0.7 (Figure S2). The pattern selection was limited to eight, as pattern beyond this shared more than 80% similarity with their neighboring patterns.

The eight SOM patterns corresponding to GEM_ERA5 based on the six-hourly smoothened pressure field closely resemble those based on ERA5, indicating consistency in the representation of synoptic-scale features (Fig. 4). The wind patterns 1-2, 3, 4, 5, 6, 7, and 8 correspond to northwesterly, westerly, southwesterly, southerly, easterly, southeasterly, and northeasterly wind directions, respectively. The distribution of pressure patterns assigned to these SOM patterns, and their associated wind regimes during the lake-ice-free period (June-November) based on GEM_ERA5, is comparable to those based on ERA reanalysis (Fig. 4 a, b). The most dominant wind direction is northwesterly, whereas southerly winds are the least frequent. The close agreement of surface winds and pressure patterns with observations provides greater confidence in the subsequent analyses based on GEM_ERA5.

### 3.2. *Water-level and wave patterns corresponding to dominant synoptic patterns and their validation*

The extreme storm events corresponding to each typical synoptic pattern based on GEM_ERA5, identified following the methodology outlined in Section 2, are listed in Table 1. Synoptic pattern 2 associated with northwesterly wind exhibits the highest wind magnitude compared to other patterns.

The coupled hydrodynamic-wave simulations corresponding to these storm events are five days in duration with the peak wind magnitude occurring on the third day in the simulation. Note that the wind magnitudes shown in Table 1 are the highest spatially averaged value for the GSL region but the wind fields used in the simulation vary in space and time. The spatial patterns of the resultant maximum significant wave height $(H_s)_{max}$ and maximum surge level $\zeta_{max}$ are shown in Figs. 5 and 6, respectively, and validated against observations (Figs. 7 and 8).

It could be noted from Fig. 5 that for synoptic patterns 1 to 4, maximum significant wave height is located at the eastern end of the main basin, driven primarily by northwesterly and westerly winds. Magnitudes of up to 4.37 m are noted for synoptic pattern 1. For synoptic patterns 5 to 8, maximum significant wave height is located in the north to northwesterly regions of GSL consistent with the easterly to southerly wind directions.

Consistent with the above, it can be seen from Fig. 6 that extreme storm events corresponding to synoptic patterns 1 to 4 mainly lead to high water levels along the southern shorelines of the main basin of GSL. This has important implications for the communities located along these shorelines, particularly Fort Resolution which is situated in this region. Among the four patterns impacting the southern shorelines, synoptic pattern 1 yields the highest storm surge of 0.61 m. By comparison, the extreme events for synoptic pattern 5 to 8 mostly cause high water levels along the western and northern shorelines of the main basin of GSL, which can impact the communities of Yellowknife and Hay River. Extreme storm event for synoptic pattern 6 produces the highest storm surge, with $\zeta_{max}$ = 0.34 m and 0.37 m at Hay River and Yellowknife, respectively.

Comparison of the simulated significant wave heights and water levels with those observed show good agreement (Figs. 7 and 8). Observed significant wave height data were available at stations C45150 and C45141 corresponding to extreme events of synoptic pattern 5 and synoptic patterns 1 to 5, respectively. The temporal evolution of $H_s$ is overall well captured (Fig. 7a), albeit some overestimations. The Root

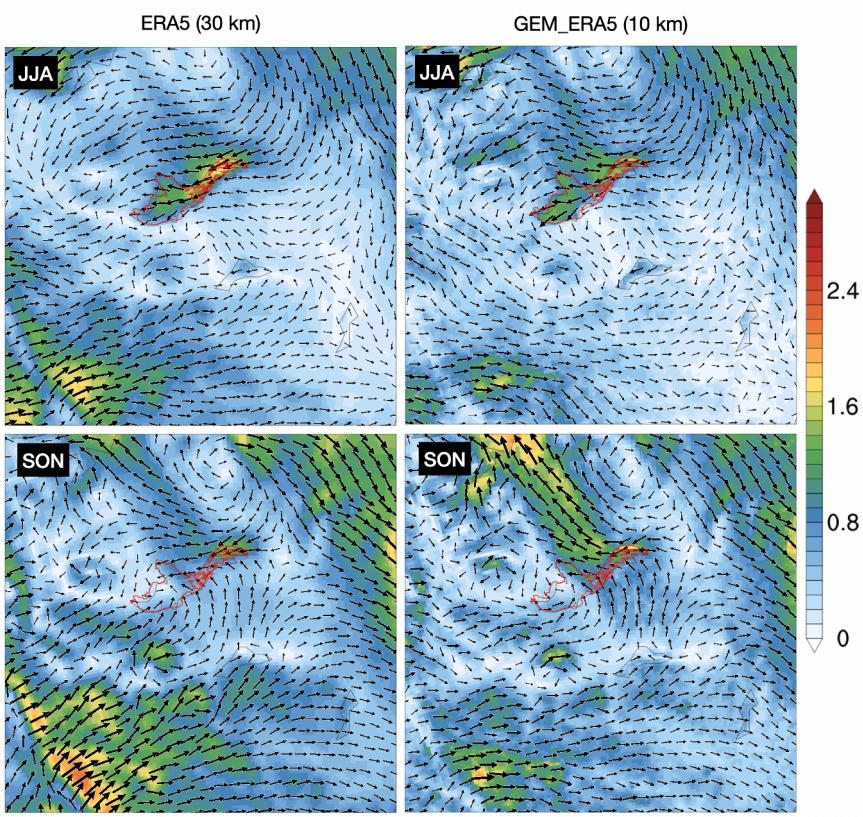


**Fig. 3.** Mean summer (JJA) and fall (SON) 10 m wind magnitudes (in $ms^{-1}$) based on ERA5 (left column) and GEM_ERA5 (right column). Also shown are the wind directions.

Mean Square Errors (RMSE) for extreme events corresponding to synoptic patterns 1-2 and synoptic patterns 4-5 are generally below 0.3 m (Fig. 7b), which is less than 10% of the observed peak $H_s$. For SOM3, RMSE is slightly higher (0.39 m).

Fig. 8 shows the comparison between the simulated and observed $\zeta$ at the Yellowknife Bay observation station. It is to be noted that the temporal resolution of observed $\zeta$ is daily, and therefore the peaks of $\zeta$ may not be well recorded, unlike the simulation, which is available at 7.5-minute frequency to ensure that the $\zeta$ peaks due to storm surges are accurately captured. Despite these differences in temporal resolution, good agreement can be noted between the observed and simulated values, with RMSE within 0.1 m for all synoptic patterns. This indicates reliable representation of the storm-surge physics by coupled Delft3D-SWAN simulation.

The general circulation patterns (refer to Figure S5 in the supplementary material), obtained by temporally averaging velocity field, reveal four gyres in the main basin, of which two are clockwise and the other two are counterclockwise. By contrast, no such clear circulation patterns exist for the east arm, primarily due to the much narrower and deeper water passages of the east arm compared with the main basin.

## 4. Typical synoptic and combined storm surge-wave patterns in future climate

In this section, projected changes to the typical synoptic patterns and related storm-surge patterns are investigated. Prior to that, GEM_MPI simulation is compared with GEM_ERA5 to understand the boundary forcing errors as discussed in Section 2. The GEM_MPI simulated surface wind (Figure S3) and synoptic patterns (Figure S4), identified by applying SOM to the MSLP fields, for the current 1991-2020 period, suggest good agreement with those based on GEM_ERA5. This suggests low boundary forcing errors, giving confidence in the future projections from GEM_MPI.

The synoptic patterns derived from the SOM analysis of GEM_MPI for the future 2041-2070 period, based on the six-hourly smoothed pressure field, closely resemble those for the current 1991-2020 period (Figure S4). Analysis of the frequency of occurrence of the synoptic patterns in current and future climates (Table 2) show some changes. Notably the frequency of occurrence of synoptic pattern 4 is projected to increase by 46%, while that of synoptic pattern 8 is projected to decrease by 20%. The frequency of occurrence of other patterns changes in the ±10% range. To fully understand the projected impact of these changes for shoreline regions, it is important to study projected changes to the intensity of extreme events for various synoptic patterns.

Projections suggest future increases in the extreme wind magnitudes over the GSL basin for synoptic patterns 1 and 3, associated with northwesterly and westerly winds. These changes correspond to enhanced pressure gradients between an intensified low over the south and a high to the north of GSL for pattern 1 and intensified low in the east of GSL for pattern 3. Pattern 1 increases in both frequency and wind magnitudes, whereas pattern 3 strengthens in wind magnitudes but becomes less frequent. Pattern 4, characterized by a low-pressure center northeast of the basin, weakens significantly but its frequency increases by approximately 46%. This pattern likely represents a decaying or displaced cyclonic system moving eastward out of the region, leaving behind a weaker pressure gradient over the lake. It is often associated with post-frontal or residual circulation rather than active storm development. The increase in frequency suggests that such weak-gradient conditions may occur more often in the future, reflecting a shift of the large-scale storm track eastward and poleward, leading to more frequent but less intense pressure systems near the northeastern basin. Extreme wind magnitude corresponding to Pattern 5, featuring a low-pressure center north of the GSL and southerly winds toward the northern shoreline, weakens slightly while its frequency declines by

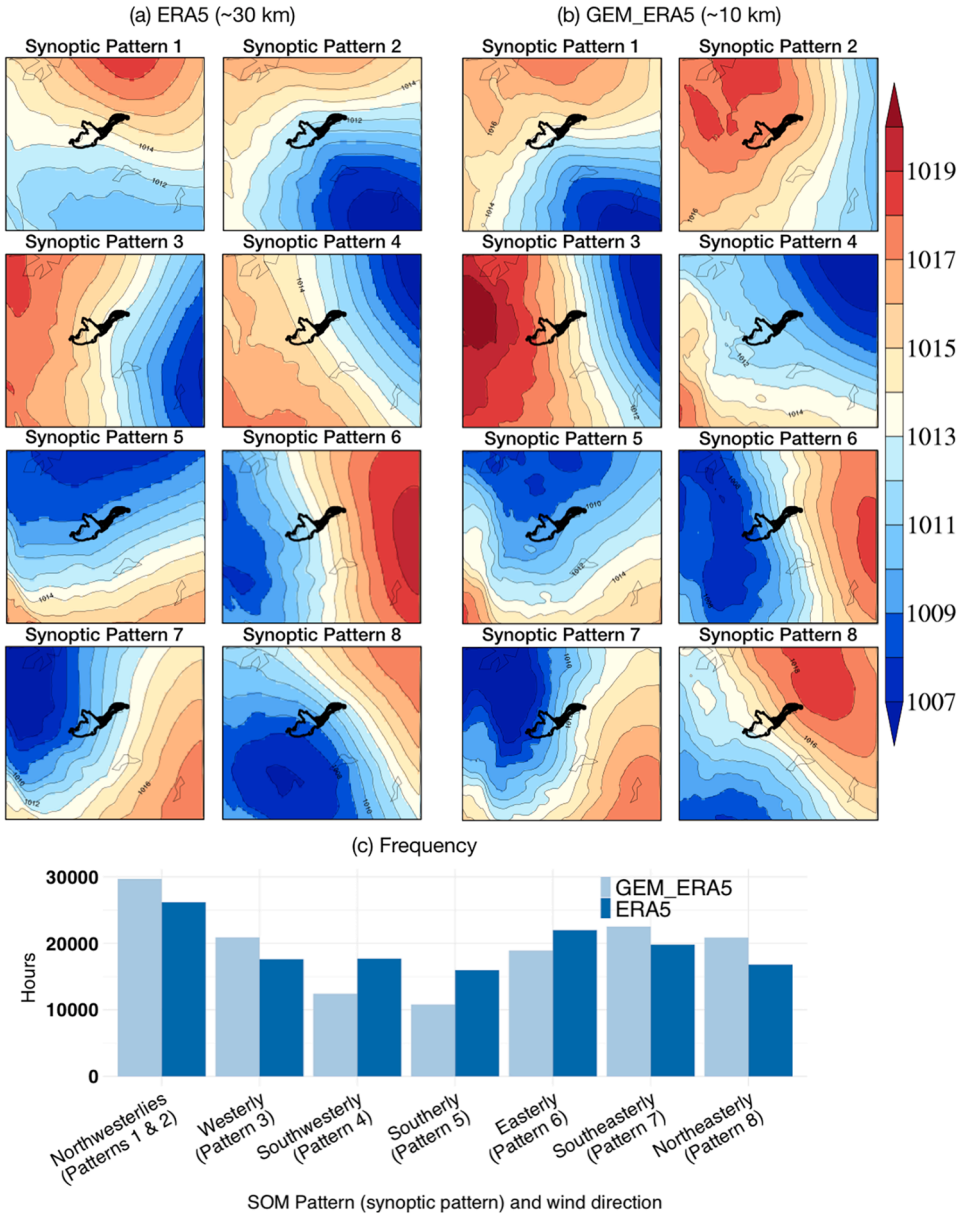


**Fig. 4.** The eight typical synoptic patterns obtained from the structural self organizing map analysis of 6-hourly smoothed MSLP fields over the analysis domain during the ice-free period (June-November) for (a) ERA5 and b) GEM _ERA5 for the current 1991-2020 period. (c) Number of hourly MSLP fields for the analysis domain that fall under the eight synoptic patterns for ERA5 and GEM_ERA5 for the current 1991-2020 period.

**Table 1**
The highest GSL-averaged wind magnitudes corresponding to synoptic patterns 1 to 8 for the Great Slave Lake, derived from GEM_ERA5 for the current (1991-2020) period.

| Synoptic pattern | Wind magnitude (m/s) |
|---|---|
| 1 | 10.2 |
| 2 | 12.6 |
| 3 | 10.2 |
| 4 | 10.5 |
| 5 | 9.73 |
| 6 | 10.1 |
| 7 | 11.4 |
| 8 | 10.3 |

about 11%. Patterns 6 (easterly winds) exhibit increased future frequency but reduced extreme wind magnitudes over the GSL basin. Pattern 7 (southeasterly winds) shows a relatively stable frequency with little change in intensity, whereas pattern 8 (northeasterly winds) exhibits a 20% decline in frequency with increased intensity. In summary, the frequency/magnitude of the extreme storms are projected to increase for synoptic patterns 1, 3 and 6 — associated with northwesterly, westerly, and easterly winds, respectively–indicating a higher potential for higher storm-surge risks for the southern shorelines, which is investigated below.

Figures S6 to S9 show the maximum surge level and significant wave height linked to extreme current and future storm events for all synoptic patterns. Storm-surge patterns driven by GEM_MPI in current climate are consistent with those driven by GEM_ERA5 shown in Fig. 6. Analysis of the surge levels for synoptic patterns individually suggest projected increases exceeding 0.4 m for the entire southern shorelines of the main GSL basin for synoptic patterns 1, 2, 3 and 6 when compared with current climate. The difference in surge level $\widehat{\zeta}_c - \widehat{\zeta}_f$ for each synoptic pattern is shown in Figure S10 of the supplementary material. Projected changes in surge level and significant wave height are generally

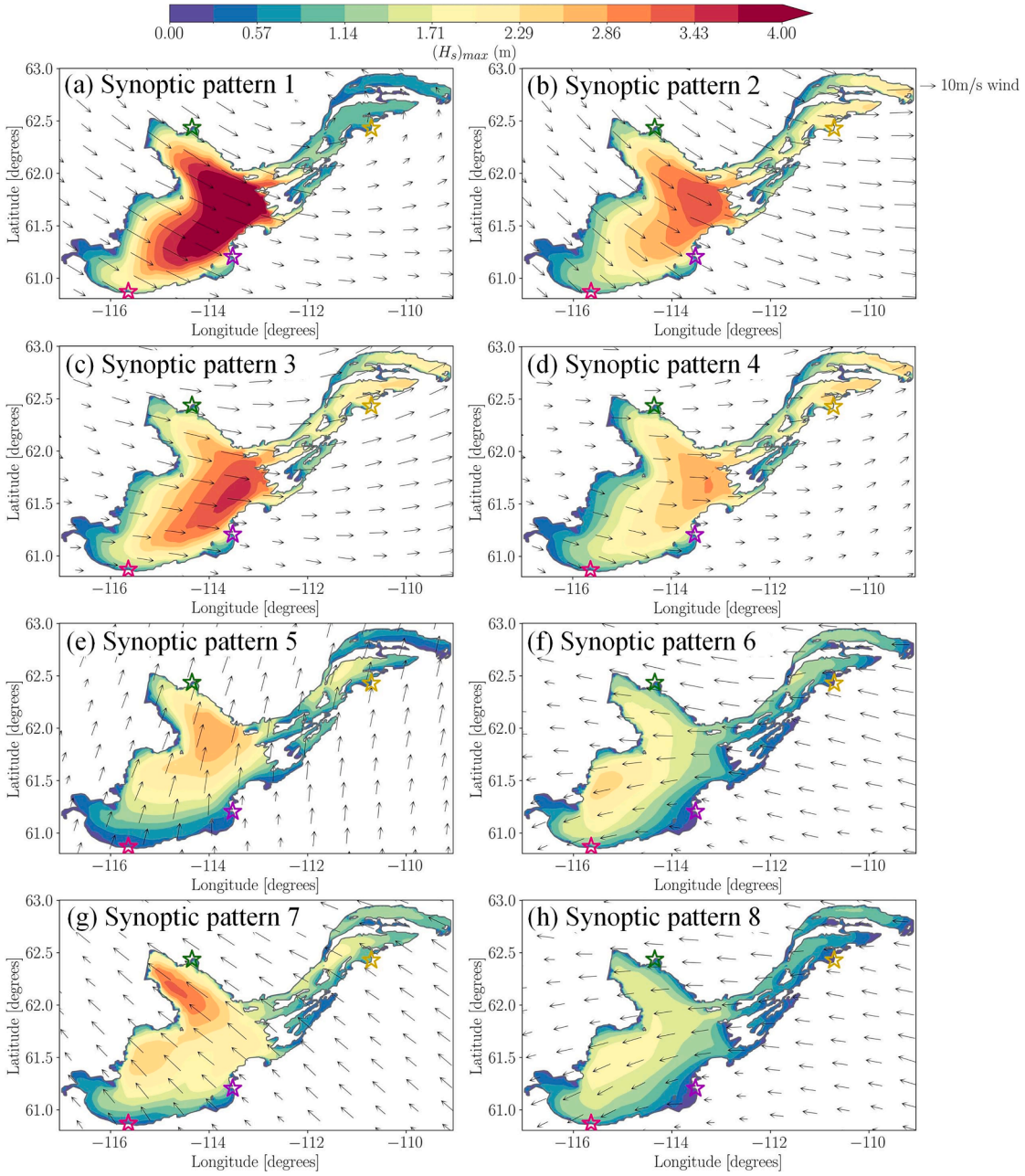


**Fig. 5.** The Delft3D-SWAN simulated highest significant wave height $(H_s)_{max}$ when driven by the extreme wind events corresponding to synoptic patterns 1 to 8 based on GEM_ERA5, for the current 1991-2020 period. The vector plot denotes the highest wind magnitude and direction. The main communities are denoted following the same notation as in Fig. 1.

consistent with the projected changes in highest wind magnitude listed in Table 2. However, for synoptic patterns 2 and 6, it is observed that although lower wind magnitude occurs in future climate, the maximum surge level and significant wave height are projected to increase. Such inconsistencies were mainly caused by the difference in wind directions associated with these two synoptic patterns. Compared with the wind direction corresponding to the maximum wind speed in current climate, the wind direction corresponding to the maximum wind speed in the future becomes more northwesterly and thus leads to higher surge levels and significant wave height. The inherent complexity of storm-surge phenomena indicates that the resultant maximum surge level is not a unique function of maximum wind speed, but rather a combined effect of maximum wind speed, wind direction, bathymetry and variation in mean-sea-level pressure.

Fig. 9 illustrates the maximum storm surges along the shoreline and their associated synoptic patterns for current and future climates, highlighting that the southern shoreline is projected to be more vulnerable in the future. Table 3 summarizes the maximum storm surge in current and future climates for the four GSL communities, showing largest projected increases at Hay River of about 59%. Fort Resolution has the highest storm surge levels among the four communities for both current and future climates. Despite having the lowest maximum storm-surge height of 0.32 m among the four communities in the future climate, Łutselk'e shows a substantial increase of about 56% compared to current climate. Fig. 9(c) and (d) suggest that the high surge levels along southern shoreline of GSL (Hay River and Fort Resolution) are mainly brought by synoptic patterns 1 and 6 for both current and future climates. High surge levels at Łutselk'e are mainly caused by synoptic patterns 3 (Fig. 9(c) and (d)). The synoptic patterns along the north-western shoreline of the main basin near Yellowknife Bay correspond to

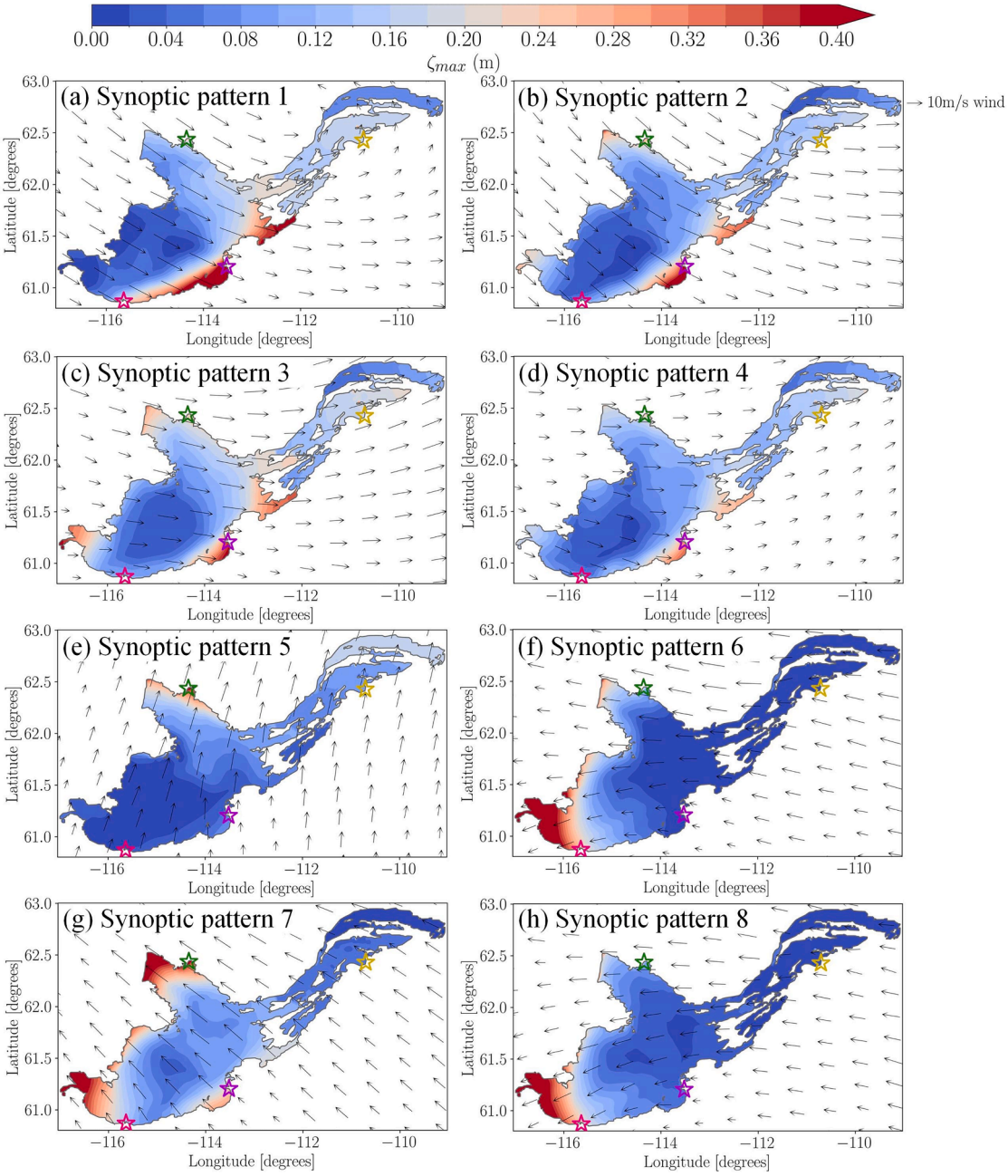


**Fig. 6.** The Delft3D-SWAN simulated highest surge levels when driven by the extreme wind events corresponding to typical synoptic patterns 1 to 8 based on GEM_ERA5, for the current 1991-2020 period. The vector plot denotes the highest wind magnitude and direction. The main communities are denoted following the same notation as in Fig. 1.

pattern 5, while those along the western shoreline are governed by patterns 6 and 7. Overall, the inundation risk along the northern and western shorelines of the basin remains nearly unchanged in the future climate, whereas the southern shoreline is projected to become more vulnerable.

## 5. Discussion

This study fills an important research gap through systematic assessment of the synoptic patterns and associated storm surge and wave characteristics for GSL. Validation of numerical results for significant wave height and surge level against observation data suggest that the RMSE is generally less than 10% of the peak values for all the synoptic patterns investigated. Furthermore, the identified synoptic patterns in current and future climates further establish a foundation for assessing maximum surge levels and vulnerability of shoreline communities, including Fort Resolution, Hay River, Yellowknife, and Łutselk'e. The relatively high wind magnitudes of the northwesterlies combined with long effective wind fetch and shallow and gently sloping shelves lead to high surge levels along the southern shores, particularly for Fort Resolution. The study suggests that Fort Resolution community will experience the highest surge levels of 0.6 m and 0.73 m in current and future climates, which warrants more detailed and higher resolution studies to determine the inundation extent.

The storm surge results presented in this study are based on a 2D hydrodynamic model. Although 2D models have been shown to be adequate in representing the hydrodynamic characteristics associated with storm surges in lakes [59,60], it is worth comparing with 3D

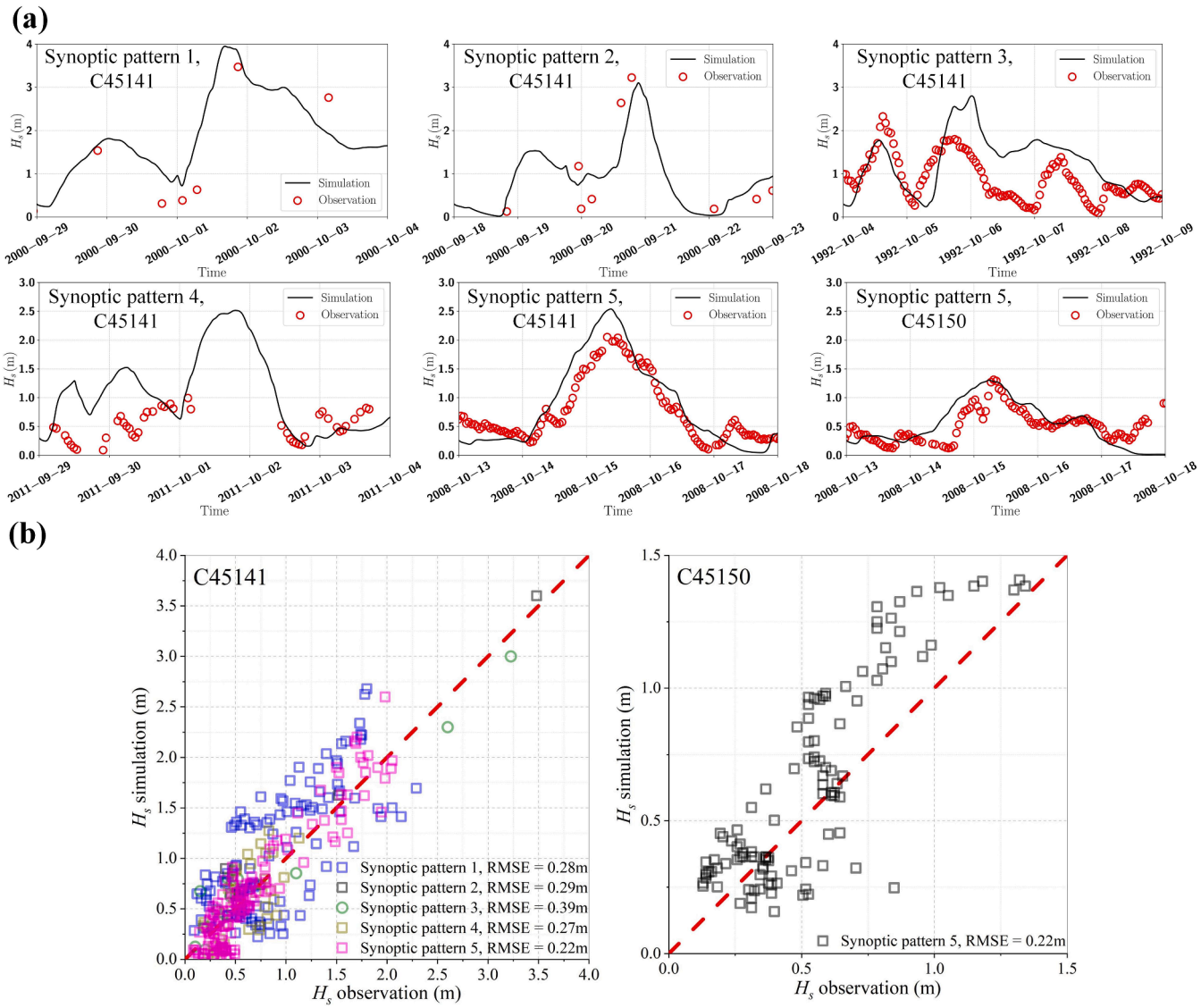


**Fig. 7.** Comparison of the observed (buoy stations C45141 and C45150) and modeled (Delft3D-SWAN simulation driven by GEM_ERA5) significant wave height $H_s$: (a) Temporal evolution of $H_s$. (b) Scatter plots of modeled vs. observed $H_s$ for observation stations C45141 (left) and C45150 (right). The RMSE for each event is shown in the figure. The red dashed lines denote the perfect fit.

models due to the inherent restrictions of the 2D model, such as the uniform-velocity approximation, oversimplified turbulence mixing and vertical shear, etc. The 3D simulation could also serve as an additional validation to the previously presented 2D simulation results validated against limited in-situ observation. Comparison of the 2D and 3D simulations for the extreme event corresponding to synoptic pattern 1 (shown in Fig. 10), using Delft3D coupled to SWAN, suggests similar patterns for the maximum water height, significant wave height and velocity fields, except for the east arm, where the 3D model predicts slightly higher surge levels and velocity than the 2D model. The circulation patterns predicted by both 2D and 3D models (Fig. 10) show consistent circulation patterns with the simulation results by León et al. [47] for the main basin. The major circulation gyre occurs in the southwestern part of the main basin while several smaller gyres form in the northern and eastern parts of the main basin. It must be noted that barotropic assumption is made in the 3D simulation, as the extreme event considered occurs in fall, when thermal stratification is negligible. Furthermore, 60 uniformly spaced layers with 8 m layer thickness in the geo-potential coordinates are considered for the 3D simulation. For extreme events in summer, it might be worthwhile considering 3D simulations in future. It must, however, be noted that the computational cost of the 3D simulation is much higher than that for the 2D simulation. For instance, the 3D simulation for synoptic pattern 1 presented here required 6 times more computational resources than the 2D simulation. Therefore, 2D simulation still serves as an attractive option for long-period simulation for storm surge.

The current study considers the lake level to be the same in current and future climates. Impact of changes in the regional hydrology on the lake level in future climate, such as changes to precipitation, evaporation, lake ice, snowmelt and runoff are not considered. It is important to understand future changes in lake levels to better quantify the impacts of storm surge. Regional climate model with 3D representation of GSL will be important for such studies which offers significant potential for improving the representation of lake–atmosphere interactions and thus the regional hydrological cycle. Such studies are available for the Laurentian Great Lakes region, such as Huziy et al. [61], where 3D hydrodynamic model NEMO (Nucleus for European Modelling of the Ocean) has been used to represent the Great Lakes. Furthermore, the synoptic and storm surge patterns presented in this study are based on outputs from a single RCM and hydrodynamic models, respectively. It would be

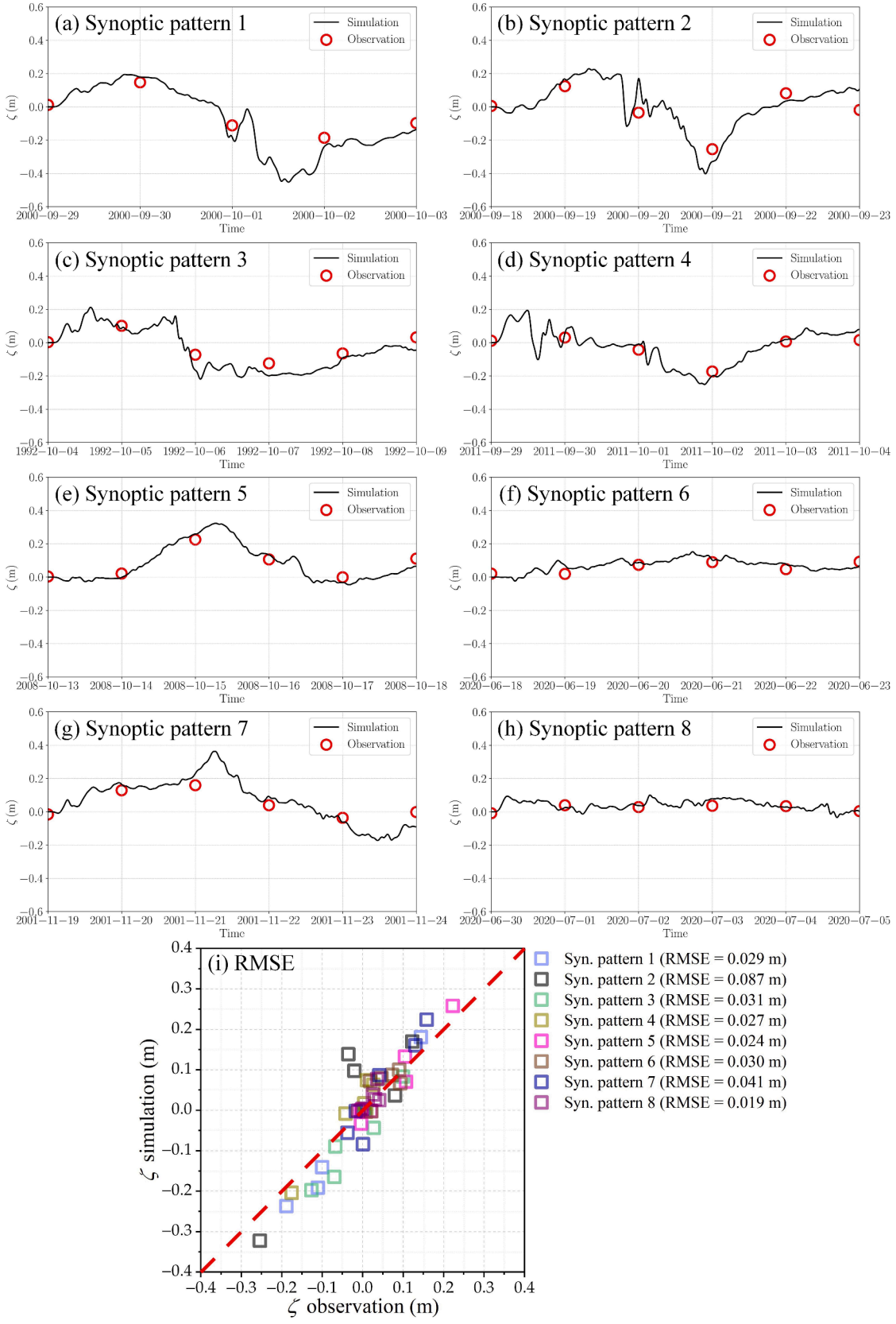


**Fig. 8.** Comparison of the observed (ECCC station) and modeled (Delft3D-SWAN simulation driven by GEM_ERA5) temporal evolution of storm surge at Yellowknife Bay (a-h). Also shown is the scatter plot of modeled vs. observed $\zeta$ (i). The RMSE for $\zeta$ is also indicated for various synoptic patterns. The red dashed line denotes perfect fit.

**Table 2**
Frequency of occurrence of synoptic patterns 1 to 8, and highest GSL-averaged wind magnitudes corresponding to these patterns for the current (1991-2020) and future (2041-2070) periods based on GEM_MPI, and their absolute and percent changes.

| Synoptic pattern | Frequency of occurrences (hours) | | | | Highest wind magnitude (m/s) | | | |
|---|---|---|---|---|---|---|---|---|
| | Current | Future | Projected changes | | Current | Future | Projected changes | |
| | | | Absolute change (hrs) | Percent change (%) | | | Absolute change (m/s) | Percent change (%) |
| 1 | 15838 | 16453 | 615 | 4 | 10.2 | 11.5 | 1.30 | 12.7 |
| 2 | 19036 | 17689 | −1347 | −7 | 12.3 | 11.7 | −0.60 | −4.88 |
| 3 | 25337 | 23959 | −1378 | −5 | 10.8 | 12.9 | 2.10 | 19.4 |
| 4 | 10500 | 15380 | 4880 | 46 | 10.2 | 8.78 | −1.42 | −13.9 |
| 5 | 14767 | 13085 | −1682 | −11 | 10.1 | 9.55 | −0.55 | −5.45 |
| 6 | 18962 | 20785 | 1823 | 10 | 10.6 | 10.0 | −0.60 | −5.66 |
| 7 | 15738 | 16067 | 329 | 2 | 11.0 | 9.07 | −1.93 | −17.5 |
| 8 | 15974 | 12734 | −3240 | −20 | 9.48 | 11.6 | 2.12 | 22.4 |

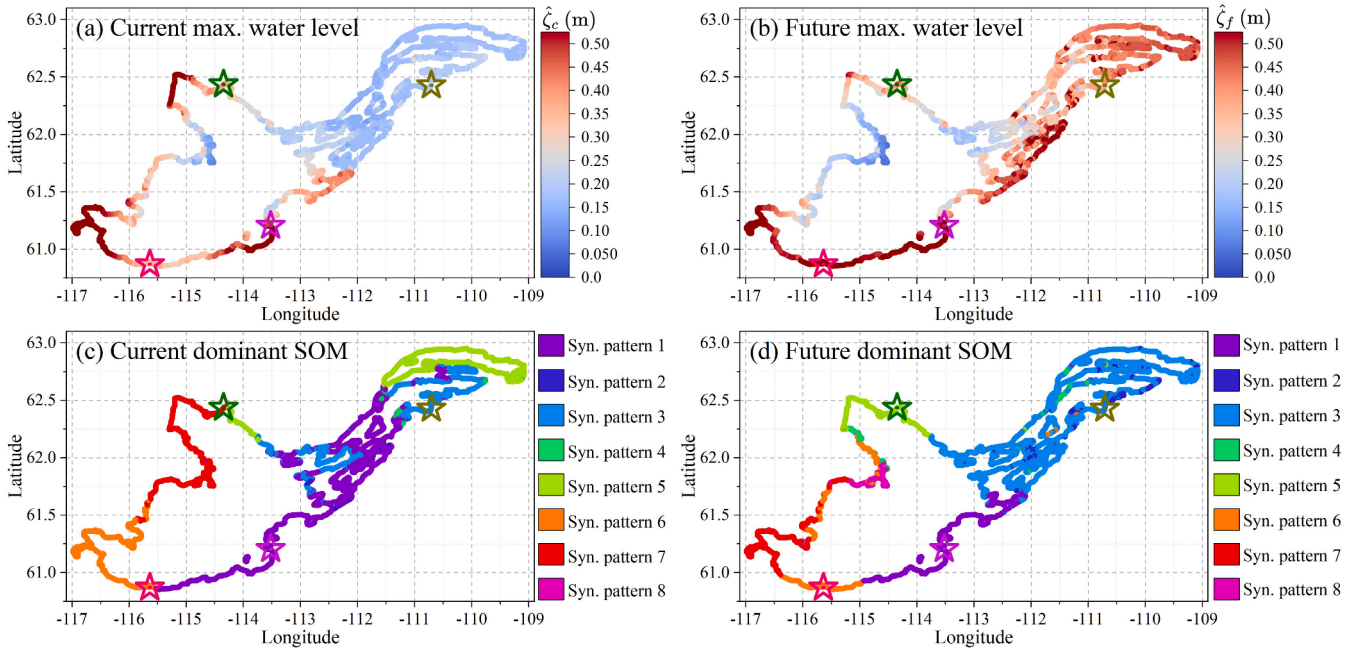


**Fig. 9.** Highest surge levels (top) and corresponding synoptic patterns (bottom) for current (left) and future (right) climates.

**Table 3**
The extreme (highest) storm surge magnitudes for current and future climates for the four communities Yellowknife, Hay River, Fort Resolution, and Łutselk'e.

| Communities | Highest storm surge (m) | | Projected changes (%) |
|---|---|---|---|
| | Current | Future | |
| Yellowknife | 0.37 | 0.45 | 18% |
| Hay River | 0.34 | 0.53 | 59% |
| Fort Resolution | 0.60 | 0.73 | 22% |
| Łutselk'e | 0.18 | 0.32 | 56% |

desirable to consider multi-model ensembles to better quantify uncertainties.

Although this study focused on the inundation potential associated with storm surges, the information generated in this study has broader practical engineering and ecological significance. For instance, significant wave heights are crucial from perspectives of safe navigation [62] and offshore infrastructure resiliency [63]. Similarly, understanding of flow patterns is important in understanding transport pathways of nutrients, contaminants and plastic debris [64,65].

## 6. Conclusions

This study, using an integrated approach combining regional climate model outputs with coupled hydrodynamic-wave models, investigates the synoptic patterns and related storm surge characteristics for the GSL for current and future climates, with the objective to identify vulnerable shoreline sections and communities. The major conclusions are summarized as follows:

- Validation of the framework consisting of RCM GEM and the two-way coupled hydrodynamic-wave model Delft3D-SWAN against available observations for the current 1991-2020 period confirm their suitability for application in transient climate simulations. Specifically, the synoptic patterns obtained through SOM analysis of MSLP fields from ERA5 and GEM_ERA5 show good agreement, which is also reflected in the wind field validation. Delft3D-SWAN simulated significant wave heights and surge levels for selected extreme events corresponding to typical synoptic patterns also show good agreement with those observed.
- The hydrodynamic simulations for the extreme events corresponding to the eight typical synoptic patterns reveal that patterns 1/2, 3 and 6 with northwesterly, westerly and northeasterly winds, respectively, impact the southern shorelines, including Fort Resolution and Hay

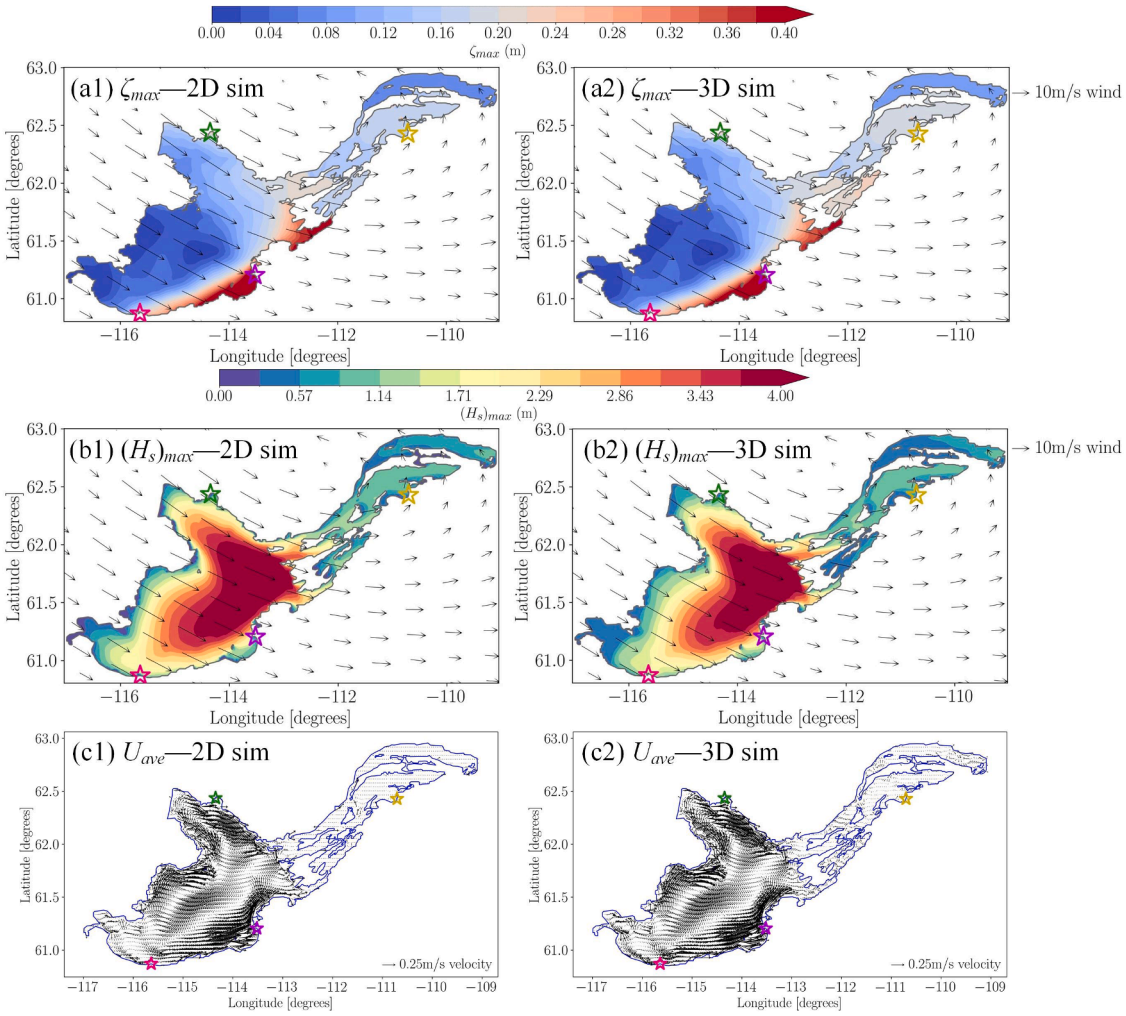


**Fig. 10.** Two-dimensional (2D; left) and three-dimensional (3D; right) simulation results based on Delft3D-SWAN for highest surge level (top panel), significant wave height (middle panel) and circulation pattern (bottom panel), corresponding to the GEM_ERA5 based extreme wind event for the first typical synoptic pattern.

River, with surges of up to 0.6 m and 0.3 m, respectively. Synoptic patterns 5 and 7 impact the northern shorelines, including Yellowknife. On the other hand, Łutselk'e on the east arm of GSL remains less affected by storm surges in current climate. The projected frequency changes for the synoptic patterns indicate a redistribution of circulation regimes over the GSL basin under future warming. The frequency of storms linked to patterns 1, 2, 3, 6 and 7 show modest changes (within ±10%); however, increases in extreme wind intensity are confined to patterns 1 and 3, enhancing wind exposure along the southern shoreline. The more frequent but weaker storms associated with pattern 4 (+46%) reflect the growing dominance of weak-gradient flow regimes tied to post-frontal or residual low-pressure systems northeast of the basin. The changes in pattern 5 indicate fewer and weaker storms, whereas pattern 8 exhibits a 20% decline in frequency with increased intensity.

- Highest projected increases in surge levels in the future climate are mainly noted for the southern shoreline and east arm of GSL, associated with future increases in extreme storm magnitudes associated with synoptic patterns 1, 3 and 6. Based on the climate-hydrodynamic-wave simulations analysed, highest surge levels at Fort Resolution and Hay River communities situated on the southern shorelines will increase 22% and 59%, respectively, under the SSP5-8.5 scenario. The increase in highest surge level at community at the east arm, Łutselk'e, is 56%. In comparison, Yellowknife located at the northern shoreline is projected to be less affected, with only 18% increase in highest surge levels associated with increase in southerly winds linked to synoptic pattern 5.

This study provides new information on storm surge characteristics for the GSL region. The robustness of the findings of this study can be further enhanced by considering multi-model ensembles considering other RCMs, driving GCMs and hydrodynamic models, and emission scenarios. Furthermore, return-level based analysis is important from infrastructure perspective, as the design climatic loads are often recommended in terms of return levels corresponding to appropriate return periods. As it is computationally expensive to undertake the coupled Delft3D-SWAN simulation for the entire 30-year current and future periods, event-based simulations considering return levels of wind magnitudes for identified synoptic patterns can be considered. These would yield much higher magnitudes of surge levels than reported in this analysis, which will be considered in future studies. Nevertheless, this study provides the foundation for undertaking such detailed studies focussed on the vulnerable regions/communities, combined with explicit inundation modelling to better quantify risks.

## CRediT authorship contribution statement

**Boyuan Yu:** Writing – original draft, Visualization, Software, Formal analysis, Data curation. **Shinto Roose:** Writing – original draft, Visualization, Validation, Software, Methodology, Formal analysis. **Laxmi**

**Sushama:** Writing – review & editing, Supervision, Project administration, Funding acquisition, Conceptualization. **Teufel Bernardo:** Writing – review & editing, Resources. **Ram Yerubandi:** Writing – review & editing, Resources.

## Declaration of competing interest

The author declares that they have no known competing financial interests or personal relationships that could have appeared to influence the work reported in this paper.

## Acknowledgments

This research was funded by the Trottier Institute for Sustainability in Engineering and Design and Environment and Climate Change Canada through a Grants and Contribution award. The simulations considered in this study were performed on the supercomputer managed by Calcul Québec and Digital Research Alliance.

## Supplementary materials

Supplementary material associated with this article can be found, in the online version, at doi:10.1016/j.rineng.2026.111612.

## Data availability

No data was used for the research described in the article.

## References

[1] IPCC, Climate Change 2021: the physical science basis, in: V. Masson-Delmotte, P. Zhai, A. Pirani, S.L. Connors, C. Péan, S. Berger, N. Caud, Y. Chen, L. Goldfarb, M.I. Gomis, M. Huang, K. Leitzell, E. Lonnoy, J.B.R. Matthews, T.K. Maycock, T. Waterfield, O. Yelekçi, R. Yu, B. Zhou (Eds.), Contribution of Working Group I to the Sixth Assessment Report of the Intergovernmental Panel on Climate Change, Cambridge University Press, 2021 (Series Ed.).

[2] S. Pattanayak, U.C. Mohanty, S.K. Dube, The storm surge prediction over Bay of Bengal and Arabian Sea: a review, Adv. Numer. Model. Data Assim. Tech. Trop. Cyclone Predict. (2016) 691–723.

[3] A. Thomas, J.C. Dietrich, T.G. Asher, M. Bell, B.O. Blanton, J.H. Copeland, R. A. Luettich, Influence of storm timing and forward speed on tides and storm surge during Hurricane Matthew, Ocean Model. 137 (2019) 1–19.

[4] M.L. Liberato, J.G. Pinto, I.F. Trigo, R.M. Trigo, Klaus–an exceptional winter storm over northern Iberia and southern France, Weather 66 (12) (2011) 330–334.

[5] N. Lin, R.E. Kopp, B.P. Horton, J.P. Donnelly, Hurricane Sandy's flood frequency increasing from year 1800 to 2100, Proc. Natl. Acad. Sci. 113 (43) (2016) 12071–12075.

[6] P. Orton, S. Vinogradov, N. Georgas, A. Blumberg, N. Lin, V. Gornitz, R. Horton, New York City panel on climate change 2015 report chapter 4: dynamic coastal flood modeling, Ann. N. Y. Acad. Sci. 1336 (1) (2015) 56–66.

[7] H.F. Needham, B.D. Keim, D. Sathiaraj, A review of tropical cyclone-generated storm surges: global data sources, observations, and impacts, Rev. Geophys. 53 (2) (2015) 545–591.

[8] S. Muis, M. Verlaan, H.C. Winsemius, J.C. Aerts, P.J. Ward, A global reanalysis of storm surges and extreme sea levels, Nat. Commun. 7 (2016) 11969, https://doi.org/10.1038/ncomms11969. Jun 27Erratum in: *Nature communications* 2016 Sep 08;7:12913. 10.1038/ncomms12913. PMID: 27346549; PMCID: PMC4931224.

[9] P. Dai, J. Nie, Robust expansion of extreme midlatitude storms under global warming, Geophys. Res. Lett. 49 (2022) e2022GL099007.

[10] N. Kohno, S.K. Dube, M. Entel, S.H.M. Fakhruddin, D. Greenslade, M.D. Leroux, N. B. Thuy, Recent progress in storm surge forecasting, Trop. Cyclone Res. Rev. 7 (2) (2018) 128–139.

[11] H. Lee, K. Calvin, D. Dasgupta, G. Krinner, A. Mukherji, P. Thorne, Y. Park, IPCC, 2023: Climate change 2023: Synthesis report, summary for policymakers. Contribution of Working Groups I, II and III to the Sixth Assessment Report of the Intergovernmental Panel on Climate Change [core writing team, H. Lee and J. Romero (eds.)], IPCC, Geneva, Switzerland, 2023.

[12] D.T. Resio, J.L. Irish, Tropical cyclone storm surge risk, Curr. Clim. Change Rep. 1 (2) (2015) 74–84.

[13] Y. Zhang, T. Zhang, A comprehensive review of assessing storm surge disasters: from traditional statistical methods to artificial intelligence-based techniques, Atmosphere 15 (3) (2024) 359.

[14] C. Chen, R.C. Beardsley, G. Cowles, J. Qi, Z. Lai, G. Gao, H. Lin, An Unstructured-Grid, Finite-Volume Community Ocean Model: FVCOM User Manual, Sea Grant College ProgramMassachusetts Institute of Technology, Cambridge, MA, USA, 2012.

[15] Deltares team, Delft3d-3d/2d modelling suite for integral water solutions hydro-morpho dynamics, User Man. 3 (2023) (2023).

[16] J.C. Warner, B. Armstrong, R. He, J.B. Zambon, Development of a coupled ocean–atmosphere–wave–sediment transport (COAWST) modeling system, Ocean Model. 35 (3) (2010) 230–244.

[17] J.E. Jones, A.M. Davies, Storm surge computations for the west coast of Britain using a finite element model (TELEMAC), Ocean Dyn. 58 (5) (2008) 337–363.

[18] V. Vallaeys, T. Kärnä, P. Delandmeter, J. Lambrechts, A.M. Baptista, E. Deleersnijder, E. Hanert, Discontinuous Galerkin modeling of the Columbia River's coupled estuary-plume dynamics, Ocean Model. 124 (2018) 111–124.

[19] Y. Zhang, A.M. Baptista, SELFE: a semi-implicit Eulerian–Lagrangian finite-element model for cross-scale ocean circulation, Ocean Model. 21 (3-4) (2008) 71–96.

[20] Y.J. Zhang, F. Ye, E.V. Stanev, S. Grashorn, Seamless cross-scale modeling with SCHISM, Ocean Model. 102 (2016) 64–81.

[21] J.J. Westerink, R.A. Luettich, A.M. Baptists, N.W. Scheffner, P. Farrar, Tide and storm surge predictions using finite element model, J. Hydraul. Eng. 118 (10) (1992) 1373–1390.

[22] J.C. Dietrich, S. Tanaka, J.J. Westerink, C.N. Dawson, R.A. Luettich Jr, M. Zijlema, H.J Westerink, Performance of the unstructured-mesh, SWAN+ ADCIRC model in computing hurricane waves and surge, J. Sci. Comput. 52 (2) (2012) 468–497.

[23] SWAN Team, SWAN Scientific and Technical Documentation, SWAN Cycle III version 41.51, Delft University of Technology, 2024.

[24] A. Roland, Y.J. Zhang, H.V. Wang, Y. Meng, Y.C. Teng, V. Maderich, U. Zanke, A fully coupled 3D wave-current interaction model on unstructured grids, J. Geophys. Res.: Oceans 117 (C11) (2012).

[25] A.F. Shchepetkin, J.C. McWilliams, The regional oceanic modeling system (ROMS): a split-explicit, free-surface, topography-following-coordinate oceanic model, Ocean Model. 9 (4) (2005) 347–404.

[26] S.C. Hsiao, H.L. Wu, W.B. Chen, C.H. Chang, L.Y. Lin, On the sensitivity of typhoon wave simulations to tidal elevation and current, J. Mar. Sci. Eng. 8 (9) (2020) 731.

[27] T.Y. Chang, H. Chen, S.C. Hsiao, H.L. Wu, W.B. Chen, Numerical analysis of the effect of binary typhoons on ocean surface waves in waters surrounding Taiwan, Front. Mar. Sci. 8 (2021) 749185.

[28] A. Baldoni, L. Melito, F. Marini, G. Galassi, P. Giacomin, G. Filomena, M. Brocchini, Modeling coastal inundation for adaptation to climate change at local scale: the case of Marche Region (central Italy), Front. Clim. 6 (2024) 1334625.

[29] M. Irani, M.M. Naderi, A.R.M. Bavani, E. Hassanzadeh, H. Moftakhari, A framework for coastal flood hazard assessment under sea level rise: application to the Persian Gulf, J. Environ. Manag. 349 (2024) 119502.

[30] P. Chittibabu, Y.R. Rao, Numerical simulation of storm surges in Lake Winnipeg, Nat. Hazards 60 (2) (2012) 181–197.

[31] D.J. Schwab, Simulation and forecasting of Lake Erie storm surges, Mon. Weather Rev. 106 (10) (1978) 1476–1487.

[32] B. Hoskins, T. Woollings, Persistent extratropical regimes and climate extremes, Curr. Clim. Change Rep. 1 (2015) 115–124, https://doi.org/10.1007/s40641-015-0020-8.

[33] E.S. Gentile, M. Zhao, K. Hodges, Poleward intensification of midlatitude extreme winds under warmer climate, NPJ Clim. Atmos. Sci. 6 (2023) 219.

[34] E.S. Gentile, L. Harris, M. Zhao, K. Hodges, Z. Tan, K.-Y. Cheng, L. Zhou, Response of extreme north Atlantic midlatitude cyclones to a warmer climate in the GFDL X-SHiELD kilometer-scale global storm-resolving model, Geophys. Res. Lett. 52 (2) (2025) e2024GL112570.

[35] Y. Ding, C. Mu, T. Wu, G. Hu, D. Zou, D. Wang, X. Wu, Increasing cryospheric hazards in a warming climate, Earth-Sci. Rev. 213 (2021) 103500.

[36] S. Rahmstorf, Rising hazard of storm-surge flooding, Proc. Natl. Acad. Sci. 114 (45) (2017) 11806–11808.

[37] N. Kramer, *Great river wood dynamics in Northern Canada* (Doctoral dissertation, Colorado State University, 2016.

[38] S. Xian, N. Lin, A. Hatzikyriakou, Storm surge damage to residential areas: a quantitative analysis for Hurricane Sandy in comparison with FEMA flood map, Nat. Hazards 79 (2015) 1867–1888.

[39] J.J. Gibson, T.D. Prowse, D.L. Peters, Hydroclimatic controls on water balance and water level variability in Great Slave Lake, Hydrol. Process.: Int. J. 20 (19) (2006) 4155–4172.

[40] J.A. Kerr, Future water levels and flows for Great Slave and Great Bear Lakes, Mackenzie River, and Mackenzie Delta. Mackenzie Basin Impact Study: Final Report, 1997, pp. 73–91.

[41] P.D. Blanken, W.R. Rouse, A.D. Culf, C. Spence, L.D. Boudreau, J.N. Jasper, D. Verseghy, Eddy covariance measurements of evaporation from Great Slave Lake, Northwest Territories, Canada, Water Resour. Res. 36 (4) (2000) 1069–1077.

[42] W.M. Schertzer, W.R. Rouse, P.D. Blanken, Cross-lake variation of physical limnological and climatological processes of Great Slave Lake, Phys. Geogr. 21 (5) (2000) 385–406.

[43] W.R. Rouse, P.D. Blanken, C.R. Duguay, C.J. Oswald, W.M. Schertzer, Climate-lake interactions. Cold Region Atmospheric and Hydrologic Studies. The Mackenzie GEWEX Experience: Volume 2: Hydrologic Processes, Springer Berlin Heidelberg, Berlin, Heidelberg, 2008, pp. 139–160.

[44] W.M. Schertzer, W.R. Rouse, P.D. Blanken, A.E. Walker, Over-lake meteorology and estimated bulk heat exchange of Great Slave Lake in 1998 and 1999, J. Hydrometeorol. 4 (4) (2003) 649–659.

[45] E. Carmack, S. Vagle, Thermobaric processes both drive and constrain seasonal ventilation in deep Great Slave Lake, Canada, J. Geophys. Res.: Earth Surf. 126 (12) (2021) e2021JF006288.

[46] León, L. F., Lam, D. C., Schertzer, W., & Swayne, D. (2006). A 3D hydrodynamic lake model: simulation on Great Slave Lake.

[47] L.F. León, D.C.L. Lam, W.M. Schertzer, D.A. Swayne, J. Imberger, Towards coupling a 3D hydrodynamic lake model with the Canadian regional climate model: simulation on Great Slave Lake, Environ. Model. Softw. 22 (6) (2007) 787–796.
[48] S.E. Howell, L.C. Brown, K.K. Kang, C.R. Duguay, Variability in ice phenology on great bear lake and great slave lake, northwest territories, Canada, from seawinds/quikscat: 2000–2006, Remote Sens. Environ. 113 (4) (2009) 816–834.
[49] K.K. Kang, C.R. Duguay, S.E.L. Howell, Estimating ice phenology on large northern lakes from AMSR-E: algorithm development and application to Great Bear Lake and Great Slave Lake, Canada, Cryosphere 6 (2) (2012) 235–254.
[50] P. Ménard, C.R. Duguay, G.M. Flato, W.R. Rouse, Simulation of ice phenology on Great Slave Lake, Northwest Territories, Canada, Hydrol. Process. 16 (18) (2002) 3691–3706.
[51] J. Côté, S. Gravel, A. Méthot, A. Patoine, M. Roch, A. Staniforth, The operational CMC–MRB global environmental multiscale (GEM) model. Part I: design considerations and formulation, Mon. Weather Rev. 126 (6) (1998) 1373–1395.
[52] H. Hersbach, B. Bell, P. Berrisford, S. Hirahara, A. Horányi, J. Muñoz-Sabater, J. N. Thépaut, The ERA5 global reanalysis, Q. J. R. Meteorol. Soc. 146 (730) (2020) 1999–2049.
[53] Q.V. Doan, H. Kusaka, T. Sato, F. Chen, S-SOM v1. 0: a structural self-organizing map algorithm for weather typing, Geosci. Model Dev. 14 (4) (2021) 2097–2111.
[54] W.M. Schertzer, Digital bathymetry of Great Slave Lake, National Water Research Institute, 2000.
[55] DFO, Marine Environmental Data Section Archive. https://meds-sdmm.dfo-mpo.gc.ca/, 2025. Ecosystem and Oceans Science, Department of Fisheries and Oceans Canada. Data, obtained on 2025/03/20.
[56] B.C. O'Neill, E. Kriegler, K.L. Ebi, et al., The roads ahead: narratives for shared socioeconomic pathways describing world futures in the 21st century, Glob. Environ. Change 42 (2017) 169–180, https://doi.org/10.1016/j.gloenvcha.2015.01.004.
[57] G. Vickers, S. Buzza, D. Schmidt, J. Mullock, The weather of the Canadian prairies, Graph. Area Forecast 32 (2001).
[58] Environment and Climate Change Canada, Arctic regional guide (En56-240/5-2017E), Government of Canada, 2017. https://publications.gc.ca/collections/collection_2017/eccc/En56-240-5-2017-1-eng.pdf.
[59] M.P. McCombs, R.P. Mulligan, L. Boegman, Y.R. Rao, Modeling surface waves and wind-driven circulation in eastern Lake Ontario during winter storms, J. Gt. Lakes Res. 40 (2014) 130–142.
[60] L.L. Swatridge, R.P. Mulligan, L. Boegman, S. Shan, Development and performance of a high-resolution surface wave and storm surge forecast model: application to a large lake, Geosci. Model Dev. 17 (21) (2024) 7751–7766.
[61] O. Huziy, B. Teufel, L. Sushama, R. Yerubandi, Heavy lake-effect snowfall changes and mechanisms for the Laurentian Great Lakes region, Atmosphere 12 (12) (2021) 1577.
[62] L. Cornejo-Bueno, J.N. Borge, E. Alexandre, K. Hessner, S. Salcedo-Sanz, Accurate estimation of significant wave height with support vector regression algorithms and marine radar images, Coast. Eng. 114 (2016) 233–243.
[63] S. Dong, M. Salauddin, S. Abolfathi, J.M. Pearson, Improved prediction of wave overtopping rates at vertical seawalls with recurve retrofitting, Ocean Eng. 302 (2024) 117647.
[64] D. Beletsky, J.H. Saylor, D.J. Schwab, Mean circulation in the Great Lakes, J. Gt. Lakes Res. 25 (1) (1999) 78–93.
[65] A.G. Driedger, H.H. Dürr, K. Mitchell, P. Van Cappellen, Plastic debris in the Laurentian Great Lakes: a review, J. Gt. Lakes Res. 41 (1) (2015) 9–19.